Solid-State Terahertz Sources Using Quantum-Well Intersubband Transitions

Paul Harrison, *Senior Member, IEEE*, Robert W. Kelsall, Kate Donovan, and Paul Kinsler

***Abstract*—In this paper, it is shown that the confined states within the conduction band of quantum-well systems have potential as sources of terahertz radiation. It is demonstrated that it is the dynamical properties of the electrons within these levels that must be manipulated in order to favor radiative emission rather than nonradiative loss. Designs are advanced for tunable emitters, optically excited lasers, and the active regions of electrically injected terahertz lasers. In the latter two device types, it is shown that the electron dynamics can be manipulated to favor population inversion at room temperature.**

***Index Terms*—Far-infrared, intersubband, quantum cascade lasers.**

I. Introduction and Theory

THE conventional approach to terahertz generation is based on oscillating currents in nonlinear electronic devices. In contrast, optically based techniques rely on electron (or hole) radiative scattering between discrete energy levels. Terahertz photons of 1–10-THz frequency can be produced with energy level separations of between 4–41 meV—an energy range that is readily accessible using the confined states in quantum-well structures.

A. Quantum Wells and Subbands

The confined levels within either the conduction or valence band of a semiconductor heterostructure have one less degree of freedom than bulk, thus giving them a two-dimensional character. While the carriers are confined along one direction, they are free to move in the other two spatial coordinates (see Fig. 1), hence, the confined levels are broadened into "subbands"—as opposed to the three-dimensional energy "bands" of bulk semiconductors.

The energy separation of subbands can be easily engineered, by altering layer thicknesses within the heterostructure to cover the majority of the infrared spectrum. Helm [1] first observed radiative emission in the mid-infrared and thus spurred an enormous interest in "intersubband transitions." Progress in this field has been rapid, with the development of the first intersubband laser in 1994 [2] and now even room-temperature devices [3]. Note these devices are "unipolar" in that they are only doped with one type of impurity (usually n-type), as opposed to traditional "interband" bipolar laser diodes, which have both n- and p-type doping.

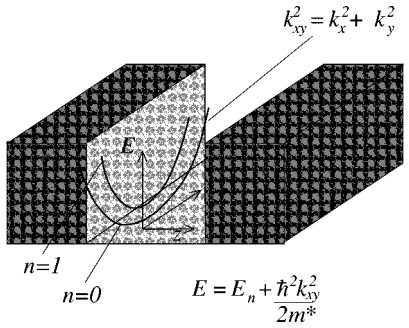

Fig. 1. Discretization of the energy levels due to the one-dimensional confinement potential of a semiconductor heterostructure, together with the broadening of the levels into "subbands" due to the in-plane (x–y) momentum of the carriers.

The extension of these developments to the far-infared or terahertz region of the spectrum is nontrivial, in that the much reduced subband separations become of the order of dominant phonons [longitudinal optic (LO) in III–V materials]. This causes an increase in the competing nonradiative scattering rates, which *can* be detrimental to radiative emission. This paper reviews the recent progress in the understanding of these scattering processes and proposes designs for both terahertz lasers and tunable emitters. In addition, recent experimental progress towards devices operating in this wavelength range will be discussed.

B. Transitions Between Subbands

Exploiting transitions between subbands (otherwise known as "*intersubband transitions*") in order to generate radiation requires an understanding of the various competing processes. For example, populating an excited state with a number of electrons (or holes) is sufficient to induce transitions to a lower energy state, as a system will always try to minimize its energy. However, only a fraction of those transitions will be radiative with the energy lost as a photon, the remainder (in fact, usually the majority) lose their energy nonradiatively by scattering with the lattice and generating a phonon.

II. Intersubband Scattering at Terahertz Subband Separations

As illustrated in Fig. 1, the subbands due to the in-plane motion of the electrons are parallel and (at low momenta) parabolic,

Manuscript received March 1, 1999; revised September 7, 1999. This work was supported by the School of Electronic and Electrical Engineering, by The University of Leeds, and by the Engineering and Physical Sciences Research Council, U.K.

P. Harrison, R. W. Kelsall, and K. Donovan are with the Institute of Microwaves and Photonics, School of Electronic and Electrical Engineering, The University of Leeds, Leeds LS2 9JT U.K. (e-mail: p.harrison@ee.leeds.ac.uk).

P. Kinsler was with the Institute of Microwaves and Photonics, School of Electronic and Electrical Engineering, The University of Leeds, Leeds LS2 9JT U.K. He is now with the Department of Applied Physics, Technical University of Delft, 2628 Delft, The Netherlands.

Publisher Item Identifier S 0018-9480(00)02533-3.

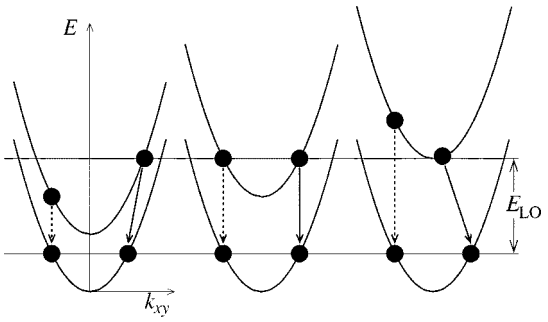

Fig. 2. Radiative (dashed, vertical) and nonradiative (solid, vertical, or diagonal) intersubband transitions for energy separations below (left-hand side), equal (center), and above (right-hand side) the LO phonon energy.

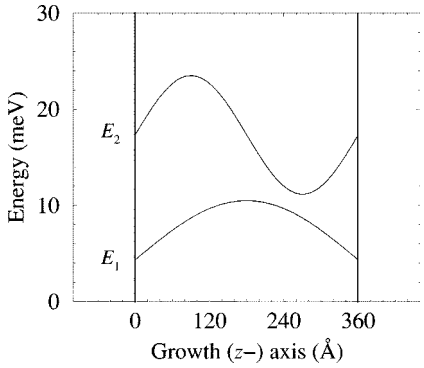

Fig. 3. Lowest two electron energy levels of a 360-Å infinitely deep GaAs quantum well.

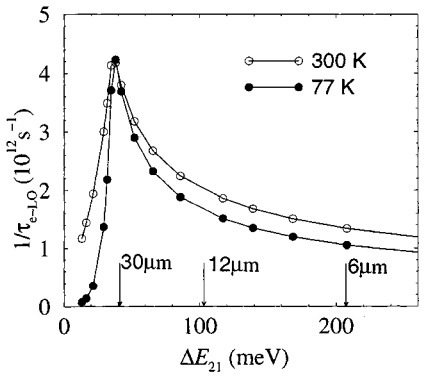

Fig. 4. Electron–LO phonon scattering rate versus energy separation between the lowest two energy levels of an infinitely deep GaAs quantum well.

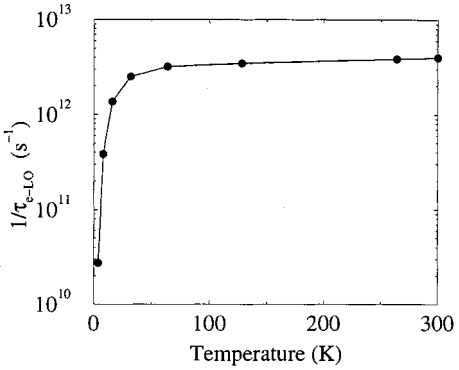

Fig. 5. Electron–LO phonon scattering rate versus temperature for a subband separation $\Delta E_{21} = 34$ meV, which is just below the LO phonon energy of 36 meV.

hence, a variety of possibilities exist for phonon and photon emission at subband separations of terahertz energies. These are illustrated schematically in Fig. 2. As photons have very little momentum, their emission causes a negligible change in the electron momentum and, hence, the radiative transitions on Fig. 2 (marked by dashed lines) are vertical. The photon does, however, have a finite energy $h\nu$ equal to the subband separation, say, $E_2 - E_1 = \Delta E_{21}$. If the subband separation is equal to that of the LO phonon (other phonon modes do exist, but in this treatise, concentration will be focused on the dominant mode), then the electron can emit a phonon and satisfy the conservation of energy with another vertical transition, as in the center diagram. This represents the generation of a low-momentum phonon and is the fastest of the three scenarios. On the other hand, if the subband separation is less than (left-hand-side diagram) or greater than (right-hand-side diagram) the LO phonon energy, then the resulting transition has to be accompanied by a momentum change. This is indicated by the diagonal (solid) lines in Fig. 2; such transitions occur slower than the former case.

A. Electron–Phonon Scattering

For illustrative purposes, an infinitely deep single GaAs quantum well is employed, the completely confined wave functions of which are displayed in Fig. 3 for a particular width of 360 Å. Such a system is useful as the subband separation ΔE_{21} can be varied, by adjusting the quantum-well width, without altering the overlap integral ($\int \psi_2(z)\psi_1(z)\,dz$), on which all the scattering rates depend. Fig. 4 displays the results of calculations of the electron–LO phonon scattering rate as a function of the subband separation, for a carrier density in each level of 10^{10} cm^{-2}. The theoretical and computational methods employed have been documented by Harrison [4].

The two main features of Fig. 4 are: 1) the scattering rate increases as the subband separation decreases through the midinfrared (6–12 μm) before peaking as ΔE_{21} equals the LO phonon energy, near the onset of the far-infrared (30 μm) and 2) below the LO phonon energy, the scattering rate is very sensitive to temperature. In terms of competing with an accompanying radiative transition, the former point is a detrimental effect when moving towards the terahertz region, however, below the LO phonon energy, this nonradiative mechanism is suppressed, particularly at low temperature.

Fig. 5 illustrates the effect of temperature on the intersubband $2 \rightarrow 1$ scattering rate for a subband separation just below the LO phonon energy. At low temperatures, as would be expected *a priori*, the electrons cannot emit phonons and, hence, the scattering rate is effectively zero. However, as the temperature increases, the scattering rate increases and, at 300K, is greater than 10^{12} s^{-1}, which implies a lifetime in the upper level of less than 1 ps. Such behavior would be very detrimental to developing emitters at or around the LO phonon energy. Fig. 6 displays the origins of this temperature sensitivity. At low temperatures, the electrons, described by Fermi–Dirac statistics, occupy all the lowest energy levels. Although an electron in the upper subband

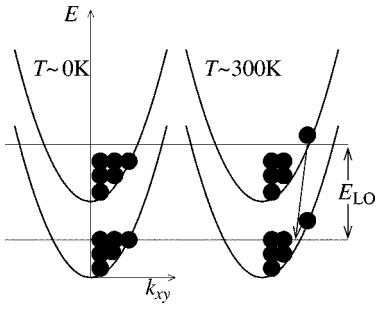

Fig. 6. Prevention of LO phonon emission at low temperatures due to Pauli exclusion, for subband separations below the LO phonon energy (left-hand side) and the activation of such processes due to the thermal broadening of the carrier distributions at elevated temperatures.

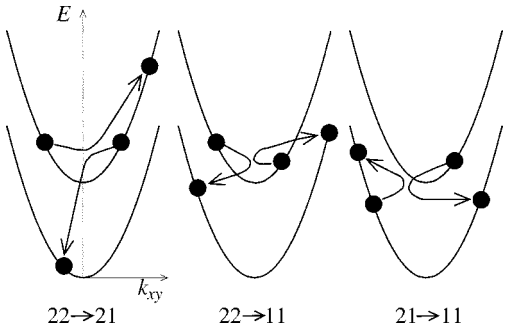

Fig. 7. Three types of intersubband electron–electron scattering.

near the top of the distribution could, in principle, undergo a diagonal transition and emit a phonon, the states to which it would scatter are all occupied and, hence, the event is prohibited (Pauli exclusion). However, at higher temperature, the electron populations broaden, creating both electrons with higher energy in the upper subband *and* empty states in the lower subband; thus, LO phonon emission is possible.

B. Electron–Electron Scattering

Electron–phonon scattering is "*inelastic*" in that the total energy of the electrons is reduced through an event. Another nonradiative mechanism is electron–electron scattering, which is "*elastic*," in that the total electron energy remains constant. As these collisions are between two electrons, then three types of events are possible, as illustrated in Fig. 7. In symmetric systems, such as the infinite quantum well being employed here, only the central event is then allowed, the $22 \rightarrow 11$, the other "Auger-type" events are parity forbidden [5].

Fig. 8 displays the results of calculations of the intersubband electron–electron scattering rate again as a function of the subband separation ΔE_{21} for the same carrier densities as before of 10^{10} cm^{-2}, which are of the order of those found in devices. For a discussion of the effect of carrier density on all the scattering rates and an explanation of the computational methods employed, see Harrison [4]. Again, it can be seen that this nonradiative rate increases as the separation between the subbands reduces from the midinfrared to the far-infrared.

C. Electron–Photon Scattering

Finally, the remaining scattering rate that is of importance is the electron–photon or radiative scattering rate itself. Fig. 9 displays the radiative *lifetime* as a function of the subband separation, calculated using the two-dimensional form of Smet *et al.* [6]. The conclusion to be drawn is that the radiative lifetime increases as the subband separation decreases, i.e., emission of photons becomes less likely.

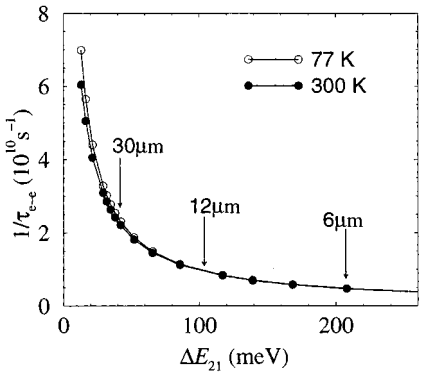

Fig. 8. Electron–electron scattering rate versus energy separation between the lowest two energy levels of an infinitely deep GaAs quantum well.

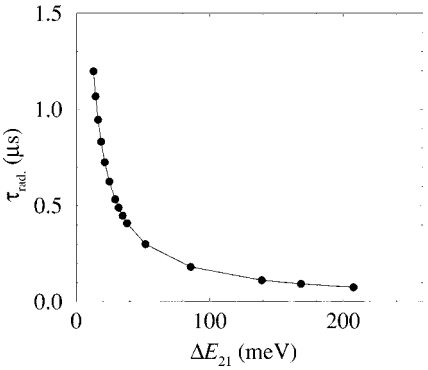

Fig. 9. Radiative lifetime versus energy separation between the lowest two energy levels of an infinitely deep GaAs quantum well.

Thus, in summary, the carrier dynamics, i.e., the behavior of the electron scattering rates, is more complex in the far-infrared than the midinfrared, due to the behavior of the electron–LO phonon scattering rate; in particular, its peak and high-temperature sensitivity at subband separations just below the LO phonon energy. In addition, the increase in the nonradiative competing mechanism of electron–electron scattering as well as the decrease in the radiative rate both suggest a reduction in the radiative efficiency of terahertz devices compared to those of the midinfrared. Despite this, progress has been made in the design of quantum-well systems to improve radiative efficiencies and, indeed, emission in the terahertz region from intersubband transitions has recently been observed [7].

III. Engineering the Scattering Rates to Favor Terahertz Emission

A. Electrically Injected Emitters

"*Electrically injected*" or "*electroluminescent*" emitters are devices whose energy input arises from injected electrons (an electric current). A terahertz emitter requires a semiconductor heterostructure in which energy level separations can be produced, which are in the range 4–41 meV (1–10 THz).

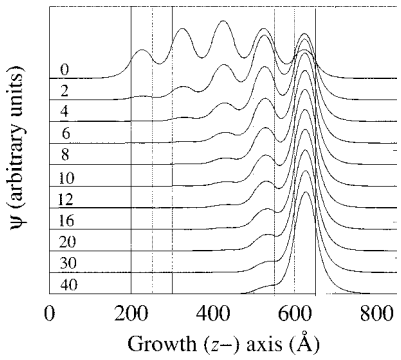

Fig. 10. Evolution of the ground state wave function on the application of an electric field (field values given on left-hand side in kV · cm^{-1}), the vertical lines mark the well-barrier interfaces.

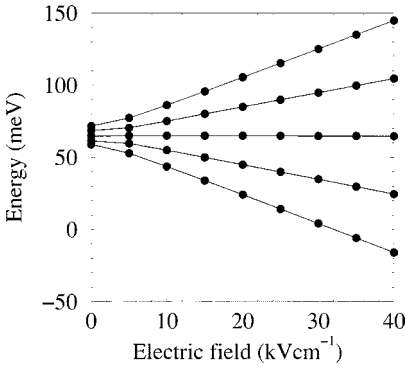

Fig. 11. Effect of the electric field on the subband separations.

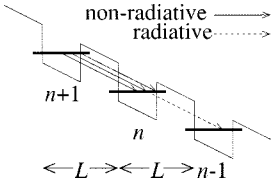

Fig. 12. Electron–phonon (nonradiative) scattering competes with photon emission (radiative scattering) as the electrons "cascade" through the energy-level "staircase."

When an electric field is applied to certain superlattices, the energy states, initially extended over the whole structure (top curve of Fig. 10), localize. At high enough fields, the state can be localized across just one or two wells (bottom curve), and from this point onwards, its energy is proportional to the field. Such a system is known as a stark ladder as the energy levels, at any field, are equally spaced. A five-well system thus produces five states, with the energy separation between the states being proportional to the field, as in Fig. 11. A superlattice in this state offers an ideal opportunity to create a *tunable* terahertz emitter, in that the emission energy $\Delta E = E_{n+1} - E_n = eFL$ is of the order of a few tens of millielectronvolts *and* is proportional to the field.

The operation of the device is illustrated schematically by Fig. 12. Electrons are injected through an electrical contact from the left-hand side at high potential, they then scatter down through the series of discrete energy levels. At each level, they can undergo either a nonradiative (electron–LO phonon or electron–electron) or radiative transition. The relative strengths

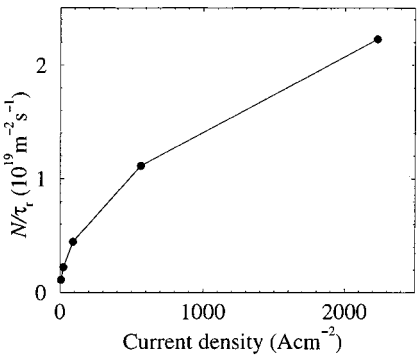

Fig. 13. Number of photons generated versus the driving current density at 4K.

of each are often summarized in terms of the "*internal quantum efficiency*," which is equal to the fraction of transitions that are radiative. Generally, in this type of device, this is quite low, of the order of 10^{-5}, which means that for every 100 000 electrons in level $n+1$, only one emits a photon when scattering down to level n. However, if the superlattice is fabricated with 100 periods (quantum wells), then the number of photons generated by 100 000 electrons passing through the complete system is 100× large, giving an internal quantum efficiency of 10^{-3}, which, although still low, is more promising.

If the superlattice is doped to provide an electron density per unit area of n (in this case, 10^{10} cm^{-2}) in each well at equilibrium operating conditions, then the current density through the device is given by $J = Ne/\tau$, where τ is the carrier lifetime in any of the levels, i.e., $(1/\tau) = (1/\tau_{e-e}) + (1/\tau_{e-\mathrm{LO}} + (1/\tau_{\mathrm{rad}})$. Correspondingly, the number of photons generated per well equals N/τ_{rad}. Fig. 13 plots this versus the current density, calculated by varying N. The data correspond to an operating electric field of 34 kV · cm^{-1}, which produces a subband separation of 34 meV, i.e., just below the LO phonon energy, it is at this point, at this low temperature of 4K that the internal quantum efficiency is highest [8]. Consider the highest current density data point at 2.2 kAcm^{-1}, this device would produce 2.1 × 10^{19} photons per unit area per unit time per well. For a mesa structure of area 1 cm^{-2} emitting photons of energy 34 meV, this then implies a peak output power of about 1 mW at a wavelength of 36 μm or 8 THz.

Transitions of this nature have recently been observed [9].

B. Optically Excited Systems

Often, if motivated by the desire for lasing from a solid-state source, the next stage in the development from an electroluminescent emitter would be an "*optically excited*" system. This offers the potential of simplifying the design of a lasing structure by removing the necessity to inject electrons though a contact and maintaining a current flow.

Lasing relies upon stimulated emission occurring within an optical cavity, which, in turn, produces the amplification. In this paper, attention will be focused on fulfilling just the first of these two criteria. A necessary condition for stimulated emission is a population inversion between two energy levels, which, in the case of an intersubband system, would imply that their must be

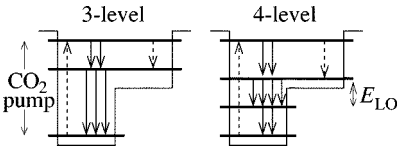

Fig. 14. Three- and four-level optically excited systems.

more electrons in the upper subband than in the lower. To sustain a population inversion, at least one other level is required.

Consider first a three-level system, the rate of change of the population of the second level could be given simplistically by the rate equation

$$\frac{dn_2}{dt} = +\frac{n_3}{\tau_{32}} - \frac{n_2}{\tau_{21}}. \tag{1}$$

When the system is at equilibrium, the population of the second level would remain constant, hence, dn_2/dt=0. Given this, then if $\tau_{32} > \tau_{21}$, i.e., if the lifetime in the second state was *less* than the lifetime of the upper state, then $n_3 > n_2$—a population inversion would exist between the third and second levels, thus fulfilling the criteria for stimulated emission.

Berger [10] proposed a three-level asymmetric quantum well as a potential design for a terahertz laser, with a population inversion between the third and second levels. Fig. 14 illustrates the mode of operation. The system is excited by the 10.6-μm line of a CO_2 laser, which excites the reservoir of carriers in the ground state to level 3. Varying the structural parameters of the quantum well allows the excitation criteria to be fulfilled, while at the same time, tuning the emission energy $E_3 - E_2$ across the terahertz region of the spectrum. Using the methods outlined above, earlier work [5], [11] has concluded a study of the scattering rates between the subbands. The population ratio τ_{32}/τ_{21} is plotted in Fig. 15 (filled symbols), for a total carrier density across all levels of 100×10^{10} cm^{-2}.

The main conclusions of which are that the population ratios peak around 5 THz, they are greater at lower temperatures, and are always less than one at 77K and 300K (though they can be greater than one at still lower temperatures). The final point implies that stimulated emission would not be observed at elevated temperatures.

Considering again the criteria for population inversion, $\tau_{32} > \tau_{21}$, if the lifetime of the lower laser level could be reduced, then the population ratio would be improved. The right-hand-side structure of Fig. 14 is an attempt at such a lifetime reduction. An additional fourth level is introduced beneath the lower laser level to enhance the scattering out (reduce the lifetime), and lasing is now designed to be between the fourth and third levels. The structural parameters of the asymmetric quantum wells were varied [11] in order to retain the resonant pump energy separation, but to hold the new level exactly, an LO phonon energy below the lower laser level, thus maximizing the effect.

Fig. 15 also displays the population ratios for these four-level systems (open symbols) [12]. It is apparent that the population ratios are much improved for both temperatures displayed and, indeed, do rise above one at the higher terahertz frequencies.

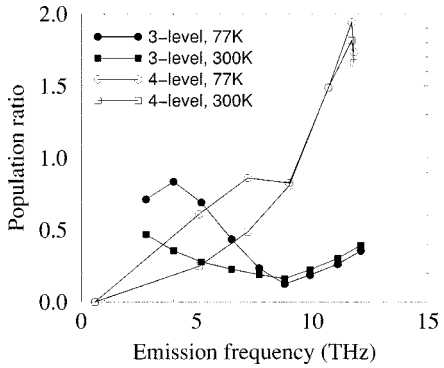

Fig. 15. Population ratio at temperatures of 77K and 300K for both the three-level and four-level systems as a function of emission energy.

C. Electrically Excited Lasers

The final stage of the design of an intersubband terahertz source is the electrically injected laser. Recalling the previous section, then simplistically population inversion is dependent upon two scattering rates, the depopulation and repopulation of a lower laser level. In a three-level system with the radiative transition between the third and second levels, then implies $(1/\tau_{21}) > (1/\tau_{32})$. As the energy of the radiative transition is fixed by the device requirements then manipulation of these rates and, hence, the population ratio τ_{32}/τ_{21} is most readily attainable by focusing attention on the depopulation of the lasing ground state.

It was found in the previous section that such an approach in optically excited systems was beneficial, with the depopulation enhanced by the addition of a level exactly an LO phonon energy below the lasing ground state. This is also an option in the active region of a quantum cascade laser, however, as pointed out by Harrison [13], depopulation at a subband anticrossing is another option.

A triple quantum well is chosen to illustrate both of these methods within the same semiconductor heterostructure. Three GaAs quantum wells of widths 56.5 Å (left-hand-side well), 96.05 Å (central well), and 84.75 Å (right-hand-side well) were separated by $Ga_{0.8}Al_{0.2}$ As barriers of width 56.5 Å. Note that the central well is the widest; thus, the eigenstate localized here is of the lowest energy, therefore, as the electric field is increased, an anticrossing with a state in a neighboring well is inevitable. This is illustrated in Fig. 16. The anticrossing between subbands 2 and 1 occurs at a field of 4 kV $\cdot$ cm^{-1}, and the subband separation is equal to the GaAs LO phonon energy of 36 meV at a field of 29 kV $\cdot$ cm^{-1}. The energy band diagram of the triple quantum well is shown in Fig. 17, along with the wave functions at the anticrossing.

In order to evaluate the potential for population inversion, the nonradiative transition rates were calculated between subbands $3 \rightarrow 2$ and $2 \rightarrow 1$ at 300 K, again for the representative carrier density of 10^{10} cm^{-2} in each level. However, because of the close proximity of subbands 2 and 1, absorption of carriers from $1 \rightarrow 2$ was significant. In fact, the transition rate from $1 \rightarrow 2$ is about 85% of the emission transition rate from $2 \rightarrow 1$. Scattering of electrons from subbands 2 to 3 also takes place, but is not as significant. Nonetheless, an exact solution of the

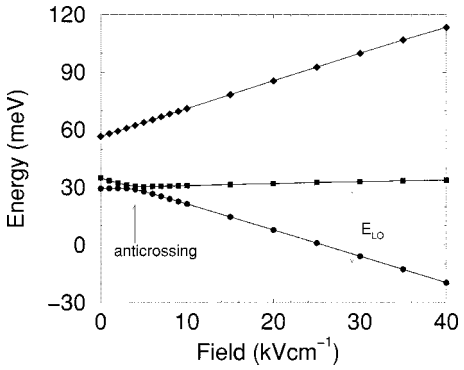

Fig. 16. Lowest three subband minima as a function of electric field.

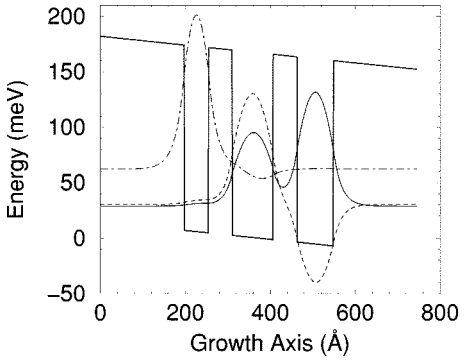

Fig. 17. Schematic diagram of the triple quantum-well structure and wave functions at the anticrossing: electric field of 4 kV $\cdot$ cm^{-1}.

subband populations for this system requires simultaneous solution of the rate equations for all three subbands. This solution must be iterated to self-consistency since the subband lifetimes τ_{ij} are themselves functions of the subband populations. However, in this study, since we know that the populations in the three subbands of the undoped active region will all be similar, we can obtain an estimate of the population ratio using the net $|3\rangle \rightarrow |2\rangle$ and $|2\rangle \rightarrow |1\rangle$ transition rates

$$\frac{n_3}{n_2} \sim \frac{\left(\frac{1}{\tau_{21}} - \frac{1}{\tau_{12}}\right)}{\left(\frac{1}{\tau_{32}} - \frac{1}{\tau_{23}}\right)}. \tag{2}$$

It must be appreciated that this is no more than a first-order approximation, but one which serves the purpose of the present study: i.e., to explore the feasibility of designing the active regions of quantum cascade structures, which can operate as lasers in the terahertz frequency range. A more sophisticated treatment to follow will include a self-consistent solution of the rate equations.

It can be seen that both the electron–LO phonon (Fig. 18) and the electron–electron (Fig. 19) transition rates peak at the anticrossing, and that the electron–LO phonon rate is a factor of five greater than the electron–electron even though the subband separation is much less than the LO phonon energy. There is also a small peak in the electron–LO emission rate at a field of 29 kV $\cdot$ cm^{-1}, where resonant LO phonon emission takes

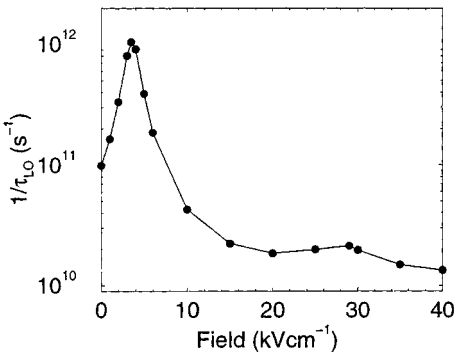

Fig. 18. Electron–LO phonon scattering rate from $|2\rangle \rightarrow |1\rangle$.

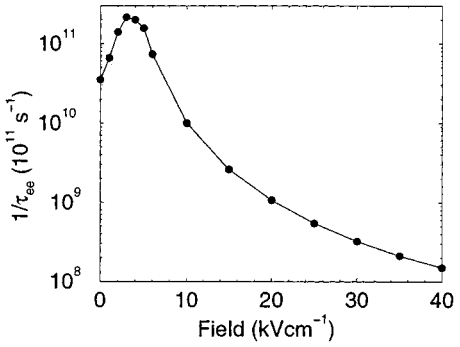

Fig. 19. Electron–electron scattering rate from $|2\rangle \rightarrow |1\rangle$.

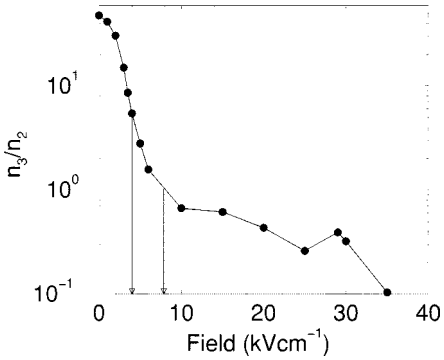

Fig. 20. Population ratio as a function of field. The viable operating range of the device is indicated by the arrows.

place for a subband separation of 36 meV. However, this resonant emission rate is almost two orders of magnitude less than the electron–LO phonon emission rate at the anticrossing.

Fig. 20 shows the effect these depopulation rates have on the overall population ratio, indeed demonstrating that a population inversion $n_3/n_2 > 1$ can exist at low fields, produced by the high electron–LO phonon and electron–electron depopulation of the lasing ground state. In addition, the figure gives an indication of the expected operating range of the device; from the subband anticrossing, with $n_3/n_2 \sim 5$, to $F = 8$ kV $\cdot$ cm^{-1}, where n_3/n_2 falls below one. Tunable emission is, therefore, possible from 39 to 33 μm. At fields below the anticrossing, the population ratio is high, but real space ordering of the energy levels prevents optical transitions between subbands 3 and 2 (the wave function associated with subband 3 is localized in

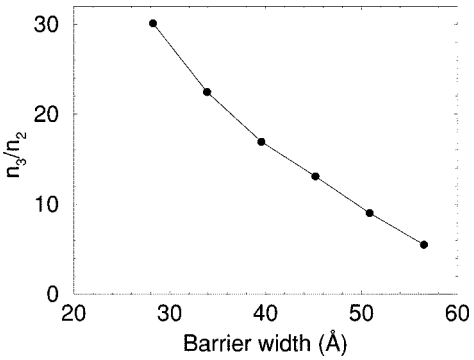

Fig. 21. Population ratio (at the anticrossing) as a function of barrier width.

the left-hand-side well and wave function associated with subband 2 is primarily localized in the right-hand-side well; see Fig. 17). The secondary peak at 29 kV $\cdot$ cm^{-1} is due to the increased depopulation due to LO phonon scattering, but is not strong enough to invert the population.

With the aim of exploring device design optimization, the barrier between the central and right-hand-side well, i.e., states $|2\rangle$ and $|1\rangle$, were decreased, the motivation being to increase the wave function overlap and, hence, the depopulation rate.

The result of this structural optimization is that the population ratio, determined at the anticrossing in each case, increases as the barrier width is reduced, as illustrated in Fig. 21, and that a population inversion of up to 30 can be achieved for a barrier width of 28.25 Å. Analysis of the scattering rates showed this is due to the increasing "nett" depopulation rate for subband 2. It may be expected that further reductions in the barrier width could lead to some "optimum" population ratio, as in the limit of the vanishing barrier, the anticrossing will disappear and, hence, the mode of operation will change. Such a scenario is the subject of ongoing investigations.

In this study, an interwell (diagonal) radiative transition has been employed; the main reasoning being to allow a triple quantum-well design that gives (almost) independent control of all three levels. Recent work [14] has shown that for far-infrared or terahertz structures, a vertical transition may give a higher internal quantum efficiency, i.e., more photons per electron. Such a vertical transition has been employed by Rochat *et al.* [15] in a double quantum-well design, from which they have observed electroluminescence (albeit very weak) at 88 μm.

IV. Conclusion

In this paper, it has been shown that energy levels of semiconductor quantum-well systems can be engineered to provide energy separations in the terahertz region of the spectrum. The potential for emitters, optically excited, and electrically injected lasers has been evaluated from the basis of the electron scattering properties. It has been shown that a superlattice could provide tunable emission at around 8 THz, albeit at low temperature. Asymmetric quantum wells have been shown to fulfill the electron dynamical criteria to exhibit population inversion at room temperature for emission around 10 THz. Furthermore, the triple quantum-well active-region designs for terahertz quantum cascade lasers have shown dynamical properties consistent with population inversion at room temperature.

References

[1] M. Helm, P. England, E. Colas, F. DeRosa, and S. J. Allen, "Intersubband emission from semiconductor superlattices excited by sequential resonant tunneling," *Phys. Rev. Lett.*, vol. 63, p. 74, 1989.

[2] J. Faist, F. Capasso, D. L. Sivco, C. Sirtori, A. L. Hutchinson, and A. Y. Cho, "Quantum cascade laser," *Science*, vol. 264, p. 553, 1994.

[3] C. Sirtori, J. Faist, F. Capasso, D. L. Sivco, A. L. Hutchinson, and A. Y. Cho, "Mid-infrared (8.5 μm) semiconductor lasers operating at room temperature," *IEEE Photon. Technol. Lett.*, vol. 9, pp. 294–296, Mar. 1997.

[4] P. Harrison, *Quantum Wells, Wires and Dots: Theoretical and Computational Physics*. New York: Wiley, 1999.

[5] P. Kinsler, P. Harrison, and R. W. Kelsall, "Intersubband electron–electron scattering in asymmetric quantum wells designed for far-infrared emission," *Phys. Rev. B, Condens. Matter*, vol. 58, pp. 4771–4778, 1998.

[6] J. H. Smet, C. G. Fonstad, and Q. Hu, "Intrawell and interwell intersubband transitions in multiple quantum wells for far-infrared sources," *J. Appl. Phys.*, vol. 79, p. 9305, 1996.

[7] B. Xu, Q. Hu, and M. R. Melloch, "Electrically pumped tunable terahertz emitter based on intersubband transition," *Appl. Phys. Lett.*, vol. 71, p. 440, 1997.

[8] K. Donovan, P. Harrison, and R. W. Kelsall, "Stark ladders as tunable far-infrared emitters," *J. Appl. Phys.*, vol. 84, pp. 5175–5179, 1998.

[9] G. Scamarcio, F. Capasso, A. L. Hutchinson, D. L. Sivco, and A. Y. Cho, "Midinfrared emission from coupled Wannier–Stark ladders in semiconductor superlattices," *Phys. Rev. B, Condens. Matter*, vol. 57, pp. R6811–6814, 1998.

[10] V. Berger, "Three-level laser based on intersubband transitions in asymmetric quantum wells: A theoretical study," *Semicond. Sci. Technol.*, vol. 9, pp. 1493–1499, 1994.

[11] P. Harrison and R. W. Kelsall, "Population inversion in optically pumped asymmetric quantum well terahertz lasers," *J. Appl. Phys.*, vol. 81, pp. 7135–7140, 1997.

[12] P. Kinsler, P. Harrison, and R. W. Kelsall, "Intersubband terahertz lasers using four-level asymmetric quantum wells," *J. Appl. Phys.*, vol. 85, pp. 23–28, 1999.

[13] P. Harrison, "Engineering the electron–phonon scattering rates in the active regions of quantum cascade lasers operating beyond 30μm," *Semicond. Sci. Technol.*, vol. 12, pp. 1487–1490, 1997.

[14] K. Donovan, P. Harrison, and R. W. Kelsall, "Comparison of the quantum efficiencies of interwell and intrawell radiative transitions in quantum cascade lasers," *Appl. Phys. Lett.*, vol. 175, pp. 1999–2001, 1999.

[15] M. Rochat, J. Faist, M. Beck, U. Oesterle, and M. Ilegems, "Far-infrared ($\lambda = 88$ μm) electroluminescence in a quantum cascade structure," *Appl. Phys. Lett.*, vol. 73, pp. 3724–3726, 1998.

Paul Harrison (M'99–SM'99) received the B.Sc. degree from the University of Hull, Hull, U.K., in 1988, and the Ph.D. degree from the University of Newcastle upon Tyne, Newcastle upon Tyne, U.K., in 1991.

Following graduation he was a Post-Doctoral Research Assistant at the University of Hull until 1995. Since 1995, he has been with the Institute of Microwaves and Photonics, School of Electronic and Electrical Engineering, The University of Leeds, Leeds, U.K., where he has been involved with ways to adapt his theoretical and computational experience in semiconductor heterostructures to terahertz sources.

Dr. Harrison received a fellowship from The University of Leeds.

Robert W. Kelsall was born in Rotherham, U.K., in 1964. He received the B.Sc. degree (with honours) and the Ph.D. degree from the University of Durham, Durham, U.K., in 1985 and 1989, respectively. His doctoral research involved studies of electronic transport in GaAs quantum wells.

From 1989 to 1993, he was a Research Assistant at the University of Durham and Newcastle-upon-Tyne, where he developed Monte Carlo simulations of MOSFET's and high electron-mobility transistors (HEMT's). In 1993, he joined The University of Leeds, Leeds, U.K., as a Lecturer in the School of Electronic and Electrical Engineering. He is currently with the Institute of Microwaves and Photonics, School of Electronic and Electrical Engineering, The University of Leeds, where he is pursuing research in the theory and simulation of advanced technology semiconductor and microwave devices.

Dr. Kelsall is a member of the Institute of Physics (U.K.).

Kate Donovan received the B.Sc. degree in physics from The University of Leeds, Leeds, U.K., in 1996, and is currently working toward the Ph.D. degree at The University of Leeds.

Her main area of interest is the theoretical study of quantum well cascade lasers.

Paul Kinsler received the B.Sc. and M.Sc. degrees from the University of Auckland, Auckland, New Zealand, and the Ph.D. degree in quantum optics from the University of Queensland, Queensland, Australia, in 1994.

He then moved into the field of semiconductors as a Post-Doctoral Research Associate at the University of Sheffield. He then joined the Institute of Microwaves and Photonics, School of Electronic and Electrical Engineering, The University of Leeds, Leeds, U.K., where he was involved with electron dynamics in semiconductor heterostructures. He is currently at the the Department of Applied Physics, Technical University of Delft, Delft, The Netherlands.